PNAS
www.pnas.org

Supplementary Information for

Long noncoding RNA LINC00673-v4 promotes aggressiveness of lung adenocarcinoma via activating WNT/β-catenin signaling

Hongyu Guan, Ting Zhu, Shanshan Wu, Shihua Liu, Bangdong Liu, Jueheng Wu, Junchao Cai, Xun Zhu, Xin Zhang, Musheng Zeng, Jun Li, Erwei Song, Mengfeng Li

Corresponding author: Mengfeng Li
Email: limf@mail.sysu.edu.cn

This PDF file includes:

Supplementary Materials and Methods
Figs. S1 to S13
Tables S1 to S15
References for SI reference citations

www.pnas.org/cgi/doi/10.1073/pnas.1900997116

Supplementary Materials and Methods

Tissue specimens and primary cell isolation. The current study was conducted on 119 LAD specimens, which were histopathologically and clinically diagnosed at the Cancer Center of Sun Yat-sen University (SYSUCC) from 2001 to 2008. These specimens are defined as the SYSUCC cohort. Clinical information regarding the research subjects is summarized in *SI Appendix*, Table S2. LAD and paired adjacent non-cancerous lung specimens were stored frozen in liquid nitrogen until further use. Adjacent non-tumor specimens were obtained from a standard distance (3 cm) from the tumor margin in resected tissues of patients with LAD who underwent surgical lung resection and confirmed by pathological diagnosis. Prior patient consents and approval from the Institutional Research Ethics Committee of Sun Yat-sen University were obtained for the use of these clinical materials for research purposes.

The preparation of LAD cells from resected samples was conducted as described previously (1). Briefly, LAD cells freshly isolated from patients were rinsed twice with PBS supplemented with penicillin/streptomycin (Gibco, Grand Island, NY) and minced with scissors. Tumor fragments were immediately put into ACL4 medium supplemented with 5% fetal bovine serum and penicillin/streptomycin. After the removal of blood clots, the tissue pieces were collected and washed with PBS containing penicillin/streptomycin, followed by suspending the cells in ACL4 medium containing 5% fetal bovine serum and penicillin/streptomycin and incubated in collagen-coated flasks.

Plasmids. Full-length LINC00673-v4 was cloned into pSin-EF2-puro retroviral vector (Addgene, Cambridge, MA). For expressing short hairpin RNA (shRNA), oligonucleotides (target sequences see *SI Appendix*, Table S12) were annealed and then

ligated into the pSuper-retro-puro plasmid to generate pSuper-LINC00673-v4-shRNA1 and pSuper-LINC00673-v4-shRNA2. The reporter plasmids containing wild-type (CCTTTGATC; TOP flash) or mutated (CCTTTGGCC; FOP flash) TCF/LEF DNA binding sites were purchased from Upstate Biotechnology (Lake Placid, NY). pCMV6-Entry-DDX3 and pCMV6-Entry-CK1ε were purchased from OriGene Technologies (Rockville, MD).

Small interfering RNAs. All siRNAs were synthesized by RiboBio (Guangzhou, China) and used at a final concentration of 10 nM. The sense strand sequences of siRNAs were summarized in *SI Appendix*, Table S12.

5' and 3' rapid amplification of cDNA ends (RACE). 5'- and 3'- RACE were performed to reveal the transcriptional initiation and termination sites of ENST00000457958.6 according to the manufacturer's instructions using SMARTer RACE 5'/3' Kit (TaKaRa, Tokyo, Japan). Briefly, total RNA was extracted from human PC9 and HCC827 cells using the Trizol reagent (Invitrogen, San Diego, CA) and treated with DNase I, followed by SMARTer first-strand cDNA synthesis to generate 5'-RACE or 3'-RACE ready cDNA. The 5'-RACE and 3'-RACE PCRs were then performed using multiple primers (*SI Appendix*, Fig. S2*B* and Table S13). PCR fragments were purified and cloned into the pMD19-T vector using the In-Fusion HD Cloning reagent provided in the kit. The plasmids containing the inserts were subsequently Sanger sequenced.

Generation of stably engineered cell lines. Plasmid pSin-LINC00673-v4 was cotransfected with pMD2G and psPAX2 packaging plasmids in 293FT cells using standard calcium phosphate transfection method (2). The two LINC00673-v4 shRNA

plasmids were transfected into the PT67, an NIH3T3-derived packaging cell line (Clontech, Mountain View, CA), using Lipofectamine 3000 reagent (Invitrogen, San Diego, CA). Subsequently, the supernatants were collected and incubated with cells to be infected for 24 h in the presence of polybrene (8 μg/ml). After infection, puromycin (1 μg/ml) was used for 10 days to select stably transduced cells.

Western blotting (WB) analysis. WB analysis was performed according to a previously described standard method (3) using antibodies anti-CK1ε and anti-DDX3 (1:1000; Bethyl Laboratories, Montgomery, TX), anti-Flag (1:2000; Sigma, St Louis, MO), anti-β-catenin, anti-TCF4, and anti-LEF1 (1:1000; Abcam, Cambridge, MA), and PCNA (1:1000; BD Biosciences, San Jose, CA). The blotted membranes were then stripped and re-blotted with anti-α-tubulin (1:2000; Sigma) mouse monoclonal antibody as a loading control.

RNA extraction and quantitative reverse transcription-PCR (qRT-PCR). Total RNA was isolated from cultured cells or surgically resected fresh LAD tissues using TRIzol (Invitrogen) according to the manufacturer's instructions. Total RNA of the formalin-fixed paraffin-embedded (FFPE) tissue sections was isolated using the RecoverAll™ Total Nucleic Acid Isolation Kit for FFPE according to the supplier's instruction. The first-strand cDNA was generated by RT using MMLV transcriptase (Promega, Madison, WI) and random primers. Real-time qRT-PCR was performed on a CFX96 real-time PCR detection system (Bio-Rad, Richmond, CA). The sequences of the primers are listed in *SI Appendix*, Table S14.

Cell nucleus/cytoplasm fraction isolation. Cell nucleus/cytoplasm fraction isolation was performed using Nuclear and Cytoplasmic Extraction Kit (Thermo, Waltham, MA)

according to the supplier's recommendation.

RNA fluorescence in situ hybridization (FISH). Cells were briefly rinsed with PBS and then fixed with 4% formaldehyde (pH 7.4) for 15 min at room temperature. Then the cells were permeabilized in 1 ml of 70% ethanol for at least 1 h at 4°C, washed in PBS 3 × 5 min at room temperature and rinsed once with 2 × saline-sodium citrate (SSC) prior to hybridization. Hybridization was carried out using anti-LINC00673 oligodeoxynucleotide probe sets (125 nM) (Exiqon, Vedbaek, Danmark) for 16 h at 37°C in a moist chamber according to the protocol from Biosearch Technologies. Subsequently, the cells were washed for 30 min in 10% deionized formamide/2×SSC at 37°C. The cells on cover-slips were counterstained with 4', 6-diamidino-2-phenylindole (DAPI), and images were obtained with a fluorescence microscope (Carl Zeiss, Oberkochen, Germany).

In situ Proximity ligation assays (PLA). Interactions between DDX3 and CK1ε were detected by *in situ* PLA. The assay was performed using Duolink® PLA Kit (Sigma) according to the supplier's instruction.

Wound healing, cell invasion, and migration assays. For wound healing assay, confluent cells in 6-well plates were pretreated with 10 μg/ml mitomycin C (Sigma) for 2 h to inhibit cell mitosis and then scratched with a pipette tip. Progression of migration was observed and photographed at indicated times. For cell invasion and migration assays, Transwell chambers (Corning) with or without coated Matrigel (BD Biosciences) were used. Indicated cells were pretreated with 10 μg/ml mitomycin C (Sigma) for 2 h, subsequently trypsinized and resuspended in DMEM without FBS. The cells were then seeded into the upper compartment of the Transwell chambers, and the lower chambers

were filled with 500 μl DMEM supplemented with 10% fetal bovine serum as a chemoattractant. After incubation for 24 h, cells having invaded to the bottom side of the inserts were fixed, stained, photographed, and quantified by counting in 5 random fields.

Analysis of gene copy number by qPCR. Genomic DNA were isolated from paraffin embedded tumor by QIAmp DNA FFPE Tissue Kit (Qiagen, Dusseldorf, Germany) following the manufacturer's instruction. Copy number gain of LINC00673 was determined by qPCR assay as previously reported (4). Primer sequences are provided in *SI Appendix*, Table S14.

ISH and Immunohistochemistry (IHC). LAD paraffin-embedded sections were dewaxed and rehydrated, then the samples were treated with proteinase K, fixed in 4% paraformaldehyde and further hybridized with 40 nM digoxin-labeled LINC00673 probe (Exiqon, sequence see *SI Appendix*, Table S15) at 55°C overnight. After incubation for 1 h at room temperature with anti-digoxin monoclonal antibody (Roche), the sections were stained with Nuclear Fast Red (2-anthracenesulfonic acid, 4-amino-9, 10-dihydro-1, 3-dihydroxy-9, 10-dioxo-, monosodium salt), mounted and examined. IHC assays were performed and quantified as previously described (5), using the following primary antibodies: anti-VEGF (1:100; Abcam), anti-MMP9 (1:100; Abcam), anti-Twist (1:100; Abcam), anti-HOXB9 (1:100; Abcam) and anti-β-catenin (1:200; Abcam). The staining scores were determined based on both the intensity and proportion of positive cells in 10 random fields. Scores representing the proportion of positively stained tumor cells in sections was graded as follows: 0, no positive cells; 1, <10%; 2, 10%-50%; and 3, >50%. The staining intensity was recorded on a scale of 0 (no staining), 1 (week staining), 2 (moderate staining), and 3 (strong staining). The staining index (SI) was calculated as

follows: SI=staining intensity × proportion of positively stained cells, resulting in scores of 0, 1, 2, 3, 4, 6, or 9. The selection of cutoff scores were based on receiver operating characteristic (ROC) curve analysis. ROC curve was generated by plotting the sensitivity and specificity of each score. The score located closest to the point with both maximum sensitivity and specificity was determined as the cutoff score (6, 7).

Northern blotting analysis. Total RNA was isolated from LAD cells and ribosomal RNA was depleted using Ribo-off rRNA Depletion Kit (Vazyme, Jiangsu, China) according to the manufacturer's instructions. Then the isolated RNA was dissolved in 2× RNA loading buffer (95% formamide, 0.025% lauryl sodium sulfate, 0.025% bromophenol blue, 0.025% xylene cyanol, 0.025% ethidium bromide and 0.5 mM edetic acid). Samples were loaded onto 15% denaturing TBE-urea gels and then transferred onto positively charged nylon membranes (Roche, Basel, Switzerland). The blotted membranes were prehybridized at 65°C for 1 h using hybridization buffer (Roche) and subjected to hybridization with digoxin-labelled DNA probe (50 μM) targeted against LINC00673 (Exiqon, Vedbaek, Danmark) overnight at room temperature. Probe (for sequence, see *SI Appendix*, Table S15) detection was performed using a digoxin Luminescent Detection Kit (Roche) according to the manufacturer's protocol. After the blots were equilibrated in detection buffer, they were incubated with the chemiluminescent substrate CDP-Star and used to expose Kodak Biomax MR film.

Co-immunoprecipitation (Co-IP). Indicated cells were washed in PBS and lysed with cell lysis buffer (25 mM HEPES, 150 mM NaCl, 1 mM EDTA, 1% NP-40, 2% Glycerol, 0.2% Cocktail, pH 7.4) supplemented with RNase inhibitor (Promega), and the lysates were then captured by 50 μl of anti-Flag magnetic beads or anti-mouse immunoglobulin

G (IgG) agarose beads (Sigma). After 24 h, the magnetic beads were washed six times with wash buffer (20 mM HEPES, 300 mM NaCl, 1 mM EDTA, 0.1% NP-40, and 0.1% Glycerol, pH 7.4). Both the input and co-IP samples were analyzed by WB analysis using anti-Flag or anti-CK1ε antibodies as described above.

RNA immunoprecipitation (RIP). RIP was performed using Magna RIP RNA-Binding Protein Immunoprecipitation Kit (Millipore, Billerica, MA) according to the manufacturer's instructions with additional UV crosslink step as described previously (8). Briefly, indicated cells in 10 ml ice-cold PBS were UV-crosslinked with 100,000 μJ/cm^2 twice (1-sec interval). Cells (2×10^7) were lysed in 100 μl RIP lysis buffer with 0.5 μl of protease inhibitor cocktail and 0.25 μl of RNase inhibitor, and supernatants were collected after centrifugation. Ten microliters of supernatant of the RIP lysate was saved as input. For each RIP, 50 μl protein G magnetic beads with 5 μg anti-DDX3, anti-CK1ε, anti-HuR, or IgG (Abcam) were prepared in a microfuge tube as instructed. One hundred microliters of supernatant of the RIP lysate was added to each beads-antibody complex in 900 μl RIP immunoprecipitation buffer (containing 860 μl RIP wash buffer, 35 μl 0.5 M EDTA and 5 μl RNase inhibitor). The samples were mixed by rotation overnight at 4°C, and the beads were then washed six times with the RIP wash buffer. Each immunoprecipitation or input sample was re-suspended in 150 μl of proteinase K buffer (107 μl of RIP Wash Buffer, 15 μl of 10% SDS, and 18 μl of proteinase K) and incubated at 55°C for 30 min with shaking to digest the protein. Samples were centrifuged, and the supernatants were collected for RNA extraction. RNA extraction was performed using TRIzol (Invitrogen) according to the manufacturers' instruction. cDNA synthesis and qPCR were performed as usual.

RNA pull-down assay. RNAs were in vitro transcribed using T7 High Yield RNA Synthesis Kit (Ambion, Austin, TX) according to the manufacturer's instructions. The transcribed RNA was labeled using RNA 3' End Biotinylation Kit (Themo, Waltham, MA), and RNA binding protein was enriched with an RNA-protein pull-down kit (Themo, Waltham, MA) according to the manufacturer's instructions. In Brief, indicated cell lysates were prepared using the Pierce^{TM} IP Lysis Buffer (protein concentration > 2mg/ml). Fifty microliters streptavidin magnetic beads were washed with 20 mM Tris (pH 7.5) twice and re-suspended by an equal volume of 1 × RNA Capture Buffer, followed by addition of 50 pmol labeled RNA to the beads and incubation at room temperature for 30 min with agitation. Antisense-LINC00673-v4 RNA was biotinylated and served as a control. The supernatant was removed and discarded, and the beads were washed twice with 20 mM Tris (pH 7.5). 1 × Protein-RNA Binding Buffer was then added to the beads and the supernatant was discarded. Subsequently, 100 µl of Master Mix (20 µl cell lysate, 10 µl 10 × Protein-RNA Binding Buffer, 30 µl 50% glycerol, and 40 µl nuclease-free water) was added to RNA-bound beads and incubated for 1 h at 4°C with rotation. The protein-RNA-beads mixture was washed with 1 × wash buffer for three times. After the wash, 50 µl of Elution Buffer was added to incubate with the beads for 30 min at 37°C with agitation. The eluted samples were boiled in SDS buffer for 5 min at 95-100°C and then the retrieved proteins were examined by Western blotting or resolved in gradient gel electrophoresis followed by mass spectrometry identification.

Luciferase reporter assay. Cells were seeded in triplicate in 48-well plates and allowed to settle for 24 hours. Indicated plasmids plus 5 ng pRL-TK-Renilla were transfected into the cells with the Lipofectamine 3000 reagent (Invitrogen, San Diego,

CA). After 48 hours, dual-luciferase reporter assay was performed using a commercial kit (Promega, Madison, WI) as previously described (9).

Tumor xenografts in vivo. All experimental procedures were approved by the Institutional Animal Care and Use Committee of Sun Yat-sen University. At least five nude mice per group were used to ensure the adequate power and each mouse with different weight was randomly allocated. For tail vein injection, 1×10^6 cells in 0.1 ml PBS were injected into the lateral tail vein of age-matched female BALB/c mice. For intracardiac injection, 1×10^5 cells were resuspended in 0.1 ml PBS and inoculated into the left cardiac ventricle of age-matched female BALB/c mice. For the antisense LNA™ GapmeRs treatment study, 1×10^6 cells in 0.1 ml PBS were injected into the lateral tail vein of age-matched female BALB/c mice. One week after injection, mice received a dose of 25 mg/kg LINC00673-v4 antisense LNA™ GapmeRs or antisense LNA™ GapmeRs negative control (PBS) weekly via tail vein injection. Metastasis was monitored by bioluminescence imaging. Briefly, mice were given D-luciferin (150 mg/kg i.v., 10 min before imaging), anaesthetized (3% isoflurane) and imaged with the Xenogen IVIS Spectrum Imaging System (Caliper Life Sciences, Hopkinton, MA). Images were analyzed with Spectrum Living Image 4.0 Software (Caliper Life Sciences). ICG-001 (Selleck Chemicals, Houston, TX), a small molecule known to inhibit Wnt/β-catenin signaling, was intraperitoneally injected at 5 mg/kg 6 days/week. At the end of observation, the mice were killed by cervical dislocation and the lungs were collected to count surface metastases under a dissecting microscope. Extracted lungs were embedded in paraffin using the routine method. Hematoxylin & eosin (H&E) staining was

performed on sections from paraffin-embedded samples for histological evidence of the tumor phenotype.

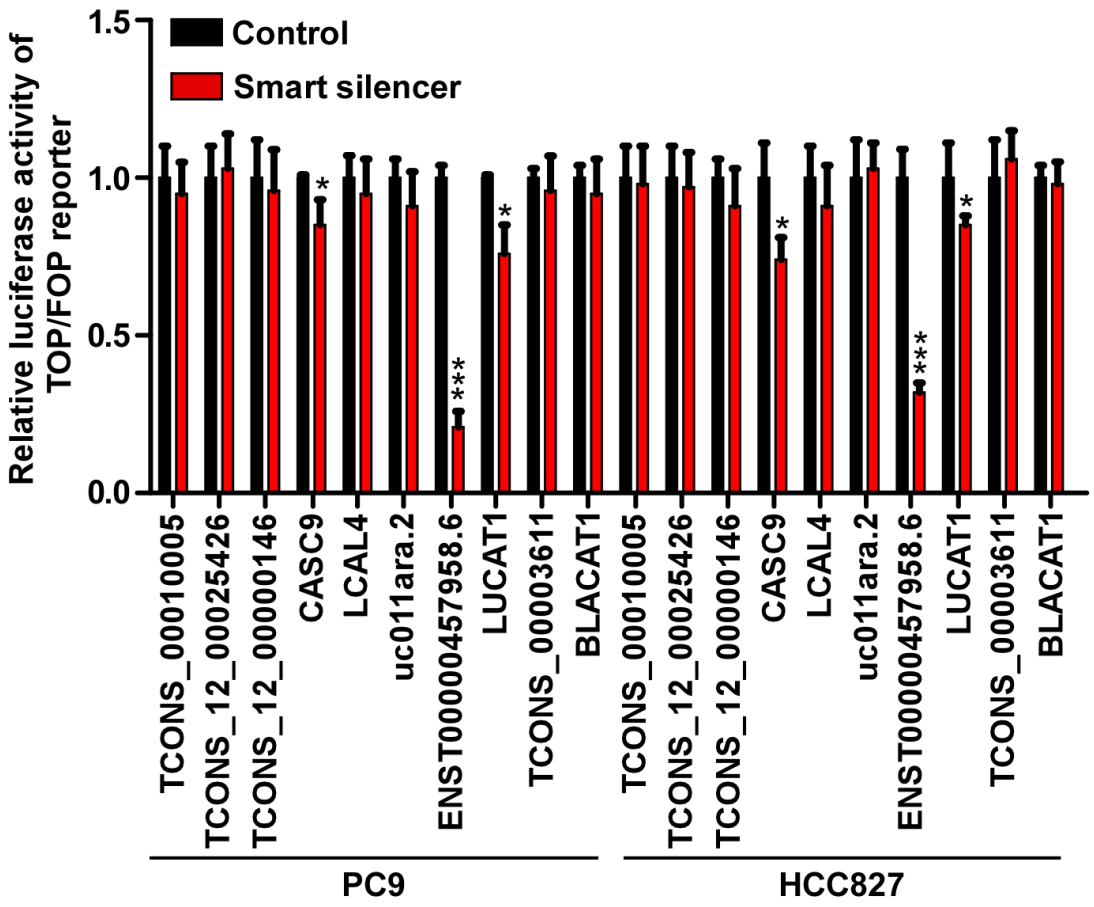

Fig. S1. Quantitative measurement of Wnt/β-catenin activation.

Reporter activity detected was normalized by Renilla luciferase activity (each bar represents the mean ± SD derived from three independent experiments, two-tailed Student's t test. **P* < 0.05, ****P* < 0.001).

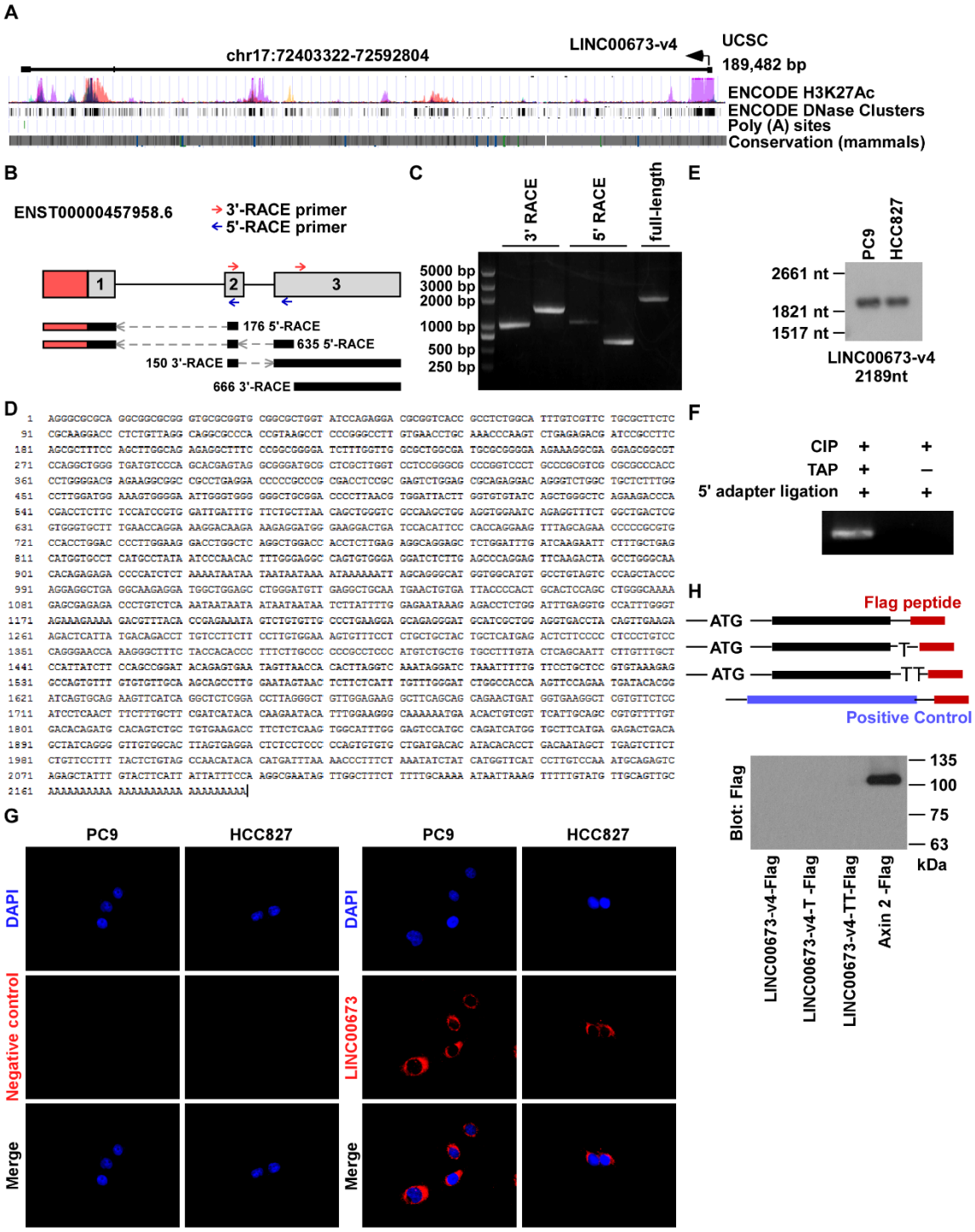

Fig. S2. Characterization of LINC00673-v4.

(A) Diagrammatic sketch of LINC00673-v4 genomic DNA structure. The transcription start site of LINC00673-v4 exhibits acetylated H3K27 (H3K27Ac) signal and DNase I

hypersensitivity. LINC00673-v4 has high evolutionary conservation in mammals. (B) Schematic overview of primers for RACE assay. (C) The images of PCR products from the 5'-RACE and 3'-RACE procedure. (D) The sequence of the full length of LINC00673-v4. (E) Northern blot analysis of the full length of LINC00673-v4. (F) LINC00673-v4 has 5’ cap structure. Total RNA was treated sequentially with Calf Intestine Alkaline Phosphatase (CIP) and Tobacco Acid Pyrophosphatase (TAP) to remove free 5’-P and the cap structure, respectively. Then a RNA adapter oligonucleotide was ligated to the RNA population (FistChoice RLM-RACE Kit, Ambion). RT-PCR was used to detect LINC00673-v4. (G) Representative images of LINC00673 expression in PC9 and HCC827 cells using RNA FISH assays. DAPI, 4’, 6-diamidino-2-phenylindole. The samples were also tested for hybridization with a LINC00673-v4 sense probe (negative control [NC]) to verify the specificity of RNA-FISH interaction. (H) Full-length of LINC00673-v4 was cloned into pcDNA3.1 with an transcription initiating codon ATG and C-terminal Flag peptide in three expression patterns. Anti-flag antibody was used to probe transcribed proteins. Axin2 with Flag tag served as a positive control.

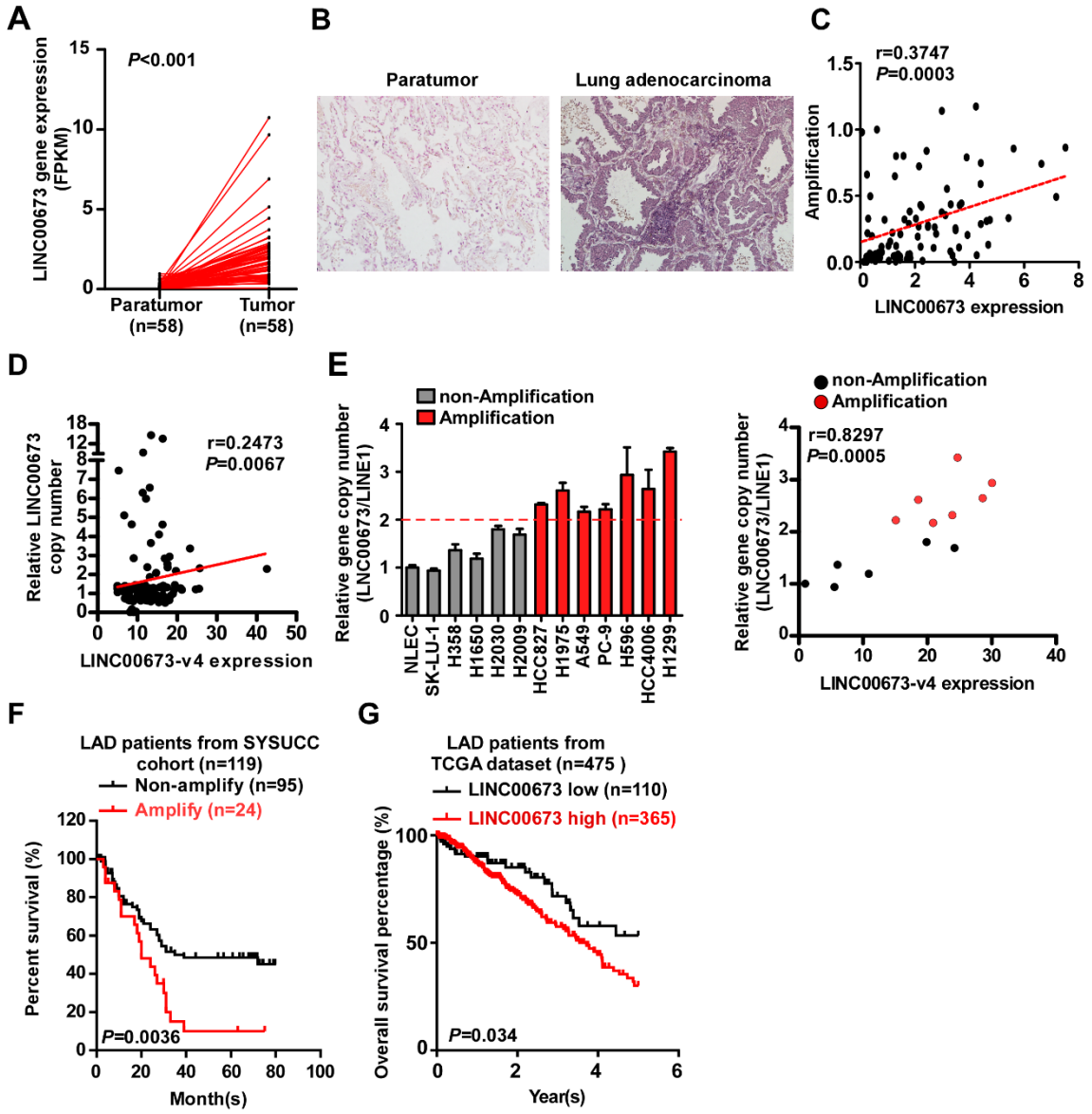

Fig. S3. LINC00673 is highly expressed in LAD.

(A) Analyses of the expression levels of LINC00673 in paired LAD and adjacent non-tumorous tissues (n=58) using TCGA dataset (two-tailed paired Student's *t* test). (B) Representative images of LINC00673 expression in SYSUCC LAD cohorts and normal lung tissues using ISH assays. (C)The expression level of LINC00673 positively correlates with its amplification status in TCGA dataset. (D and E) Correlation analysis between amplification status of LINC00673 and its expression in the SYSUCC cohort

(D) and LAD cell lines (E) (Correlation was assessed using Spearman correlation coefficient). (F) Kaplan-Meier survival analysis of LAD patients in the SYSUCC cohort stratified by LINC00673-v4 genomic amplification status. The selection of cutoff scores were based on receiver operating characteristic (ROC) curve analysis. (G) Overall survival was assessed in patients with LAD using the TCGA dataset. Determination of the optimal cutoff value for predicting survival was performed by using X-tile bioinformatics software version 3.6.1.

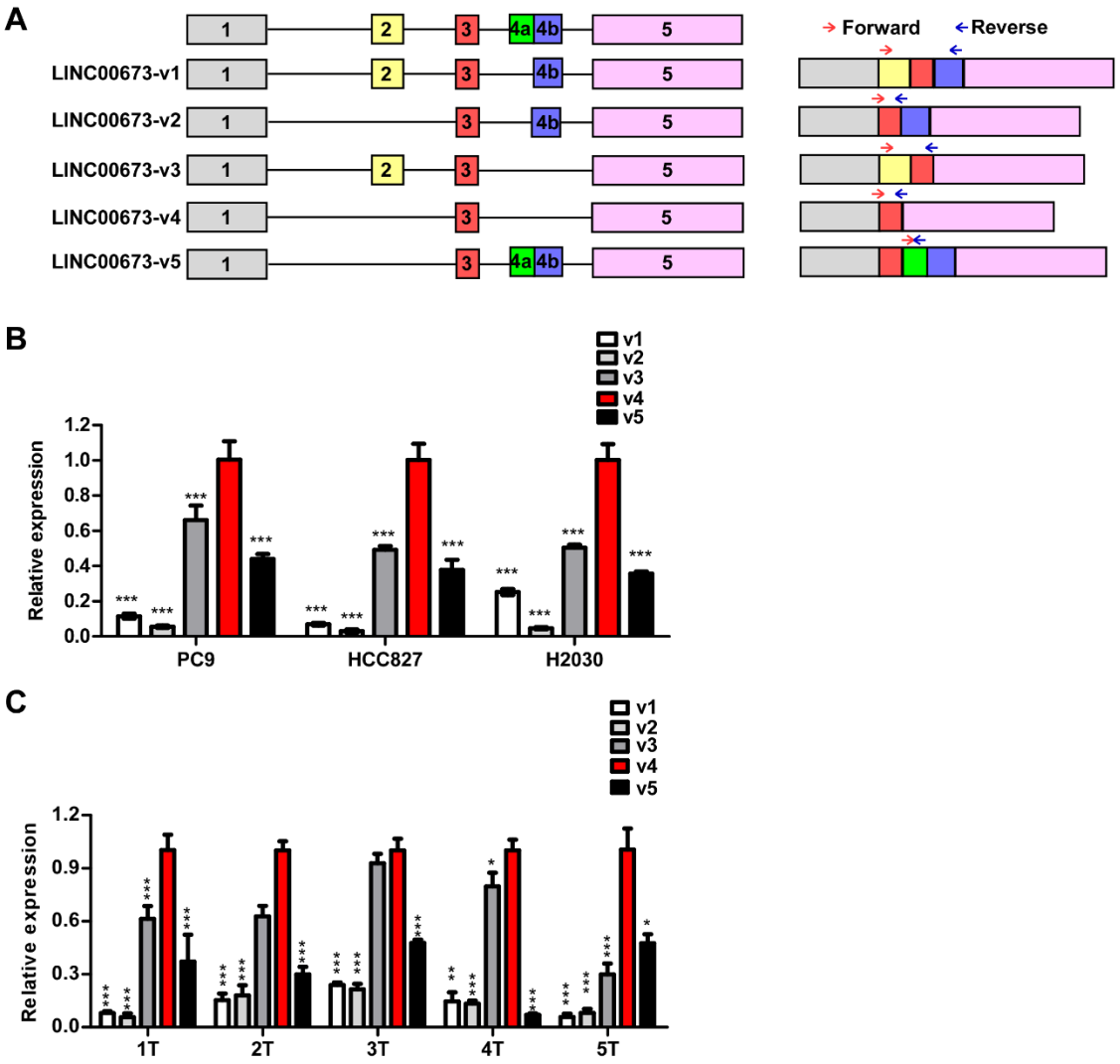

Fig. S4. Abundance of transcript variants of LINC00673 in LAD.

(A) Schematic overview of variant-specific primers for LINC00673. (B and C) Abundance of transcript variants of LINC00673 in PC9, HCC827, and H2030 LAD cell lines (B) and LAD specimens (C) (each bar represents the mean ± SD derived from three experiments, one-way ANOVA followed by Dunnett's multiple comparison test. **P* < 0.05, ***P* < 0.01, ****P* < 0.001).

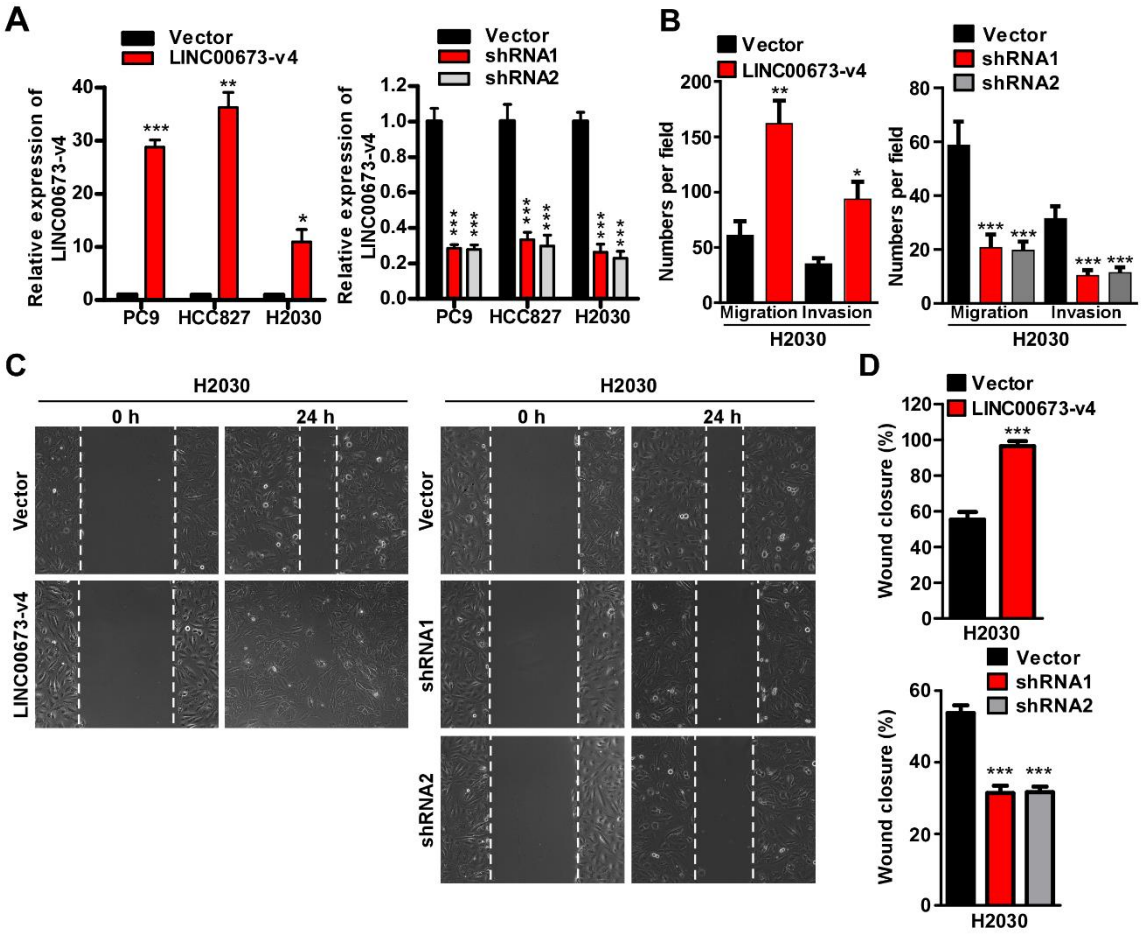

Fig. S5. LINC00673-v4 regulates LAD cell invasion and migration *in vitro*.

(A) PC9, HCC827 and NCI-H2030 cell lines stably transduced with ectopic LINC00673-v4 or knocked down for LINC00673-v4 were constructed (left: each bar represents the mean ± SD derived from three independent experiments, two-tailed Student's t test; right: each bar represents the mean ± SD derived from three experiments, one-way ANOVA followed by Dunnett's multiple comparison test. **P* < 0.05, ***P* < 0.01, ****P* < 0.001). (B) Quantification of indicated invading or migrating cells analyzed by Matrigel-coated or -noncoated Transwell assays, respectively (left: each bar represents the mean ± SD derived from three independent experiments, two-tailed Student's t test; right: each bar represents the mean ± SD derived from three experiments, one-way ANOVA followed by

Dunnett's multiple comparison test. *$P < 0.05$, **$P < 0.01$, ***$P < 0.001$). (C) Representative micrographs of wound healing assay of indicated cells. Wound closures were photographed at indicated time after wounding. (D) Quantification of wound closures of the indicated cells (up: each bar represents the mean ± SD derived from three independent experiments, two-tailed Student's t test; down: each bar represents the mean ± SD derived from three experiments, one-way ANOVA followed by Dunnett's multiple comparison test. ***$P < 0.001$).

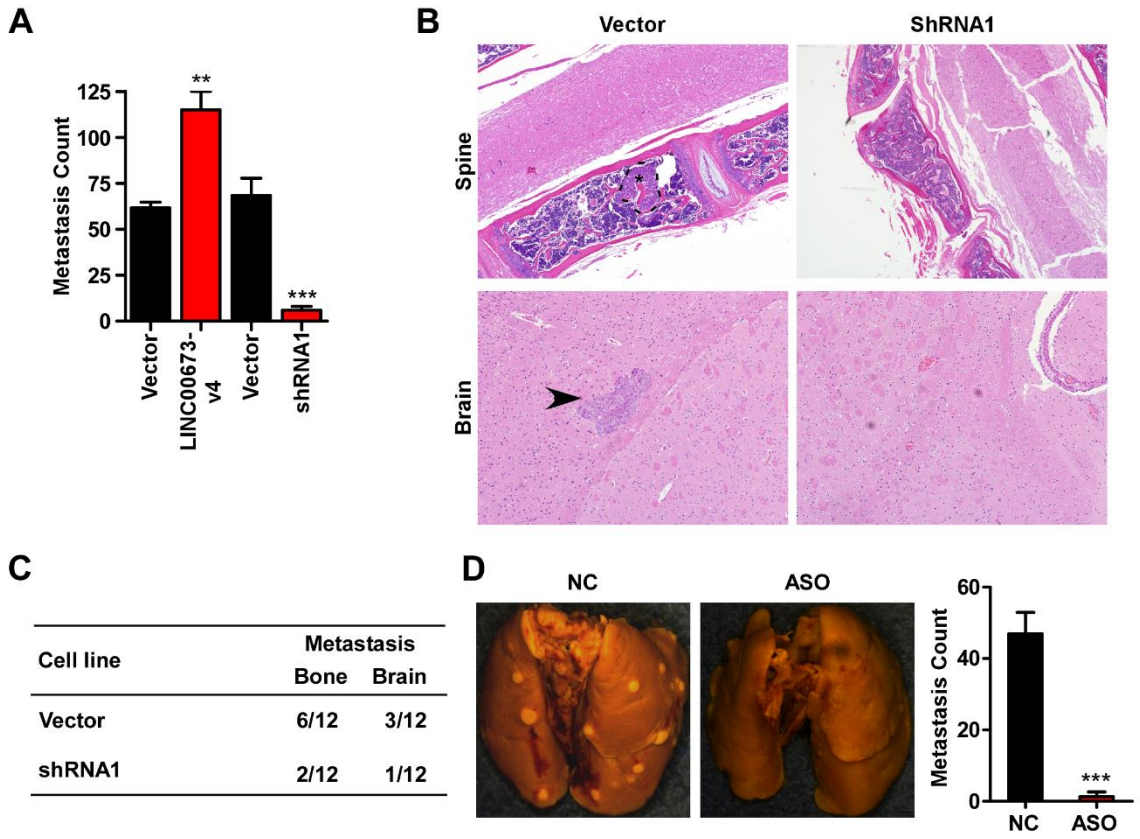

Cell line	Metastasis	
	Bone	Brain
Vector	6/12	3/12
shRNA1	2/12	1/12

Fig. S6. LINC00673-v4 promotes LAD cell metastasis.

(A) Number of visible surface metastatic lesions in mice (n = 5 per group) receiving tail vein injection of indicated cells (each bar represents the mean ± SD, two-tailed Student's t test. **P* < 0.05, ***P* < 0.01, ****P* < 0.001). (B) Metastatic bone and brain lesions in mice were confirmed by H&E staining. (C) The number of mice in which the metastatic lesions were detected is summarized. (D) Representative bright-field imaging of the lungs are shown (left). Number of visible surface metastatic lesions in mice (n = 10 per group) (right, two-tailed Student's t test, ****P* < 0.001).

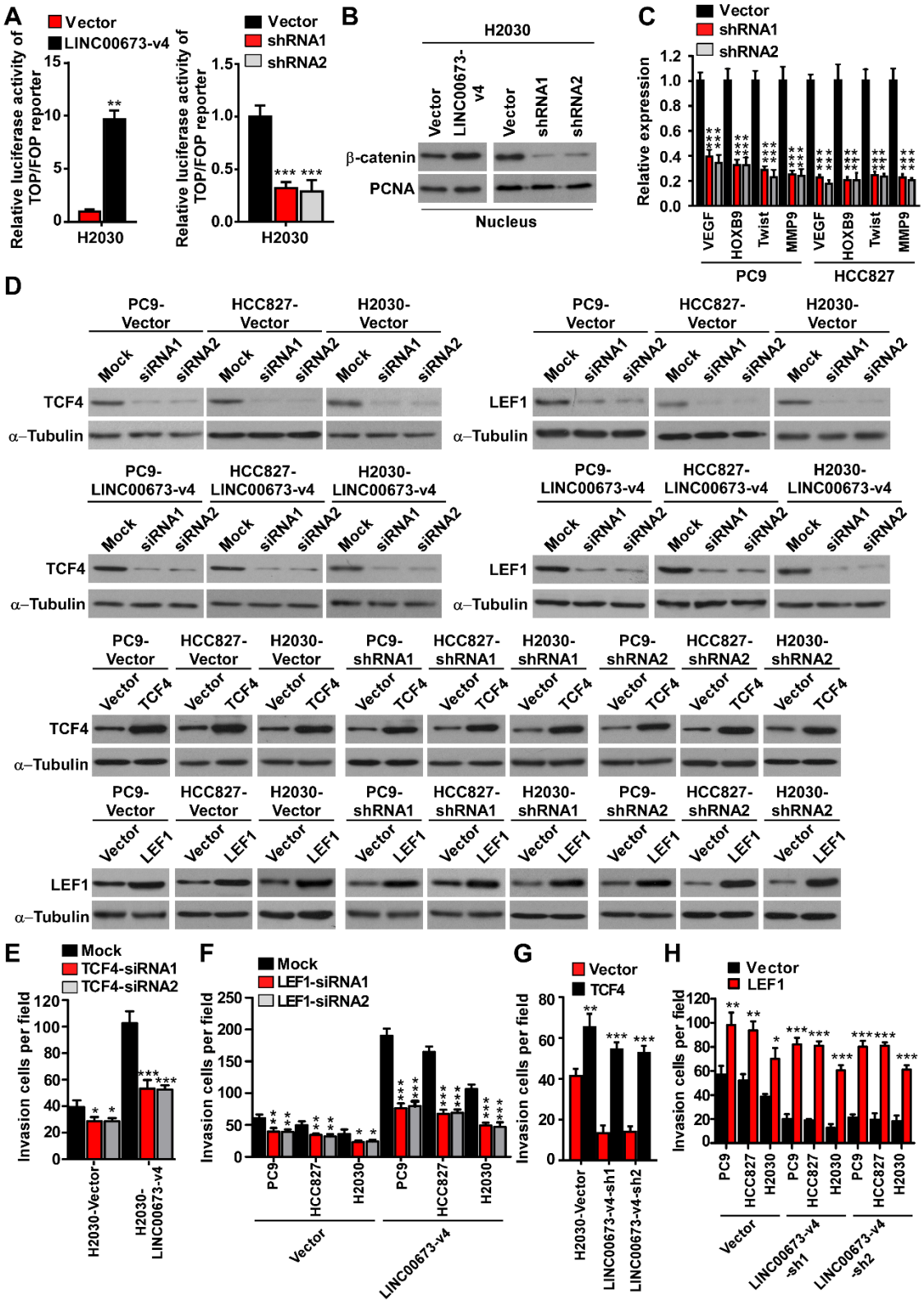

Fig. S7. LINC00673-v4 activates WNT/β-catenin signaling.

(A) NCI-H2030 cells were transfected with TOP-flash or FOP-flash and Renilla pRL-TK plasmids, and dual-luciferase assays were performed 48 h after transfection. The reporter activity was normalized by Renilla luciferase activity (left: each bar represents the mean ± SD derived from three independent experiments, two-tailed Student's t test; right: each bar represents the mean ± SD derived from three experiments, one-way ANOVA followed by Dunnett's multiple comparison test. $^{**}P < 0.01$, $^{***}P < 0.001$). (B) Altered nuclear translocation of β-catenin in response to LINC00673-v4 overexpression in NCI-H2030 cells were analyzed by WB analysis. (C) The expression levels of MMP9, Twist, VEGF, and HOXB9 were decreased by silencing of LINC00673-v4 (each bar represents the mean ± SD derived from three experiments, one-way ANOVA followed by Dunnett's multiple comparison test. $^{***}P < 0.001$) in LAD cells. (D) Expression levels of TCF4 and LEF1 in indicated cells were analyzed by WB. (E and F) Quantification of invading cells using Transwell invasion assay in LINC00673-v4-overexpressing and vector-control cells with silencing of TCF4 (E) or LEF1 (F) (each bar represents the mean ± SD derived from three experiments, one-way ANOVA followed by Dunnett's multiple comparison test. $^{*}P < 0.05$, $^{**}P < 0.01$, $^{***}P < 0.001$). (G and H) Quantification of invading cells by overexpression of TCF4 (G) or LEF1 (H) in LINC00673-v4-silencing and vector-control cells (each bar represents the mean ± SD derived from three independent experiments, two-tailed Student's t test. $^{*}P < 0.05$, $^{**}P < 0.01$, $^{***}P < 0.001$).

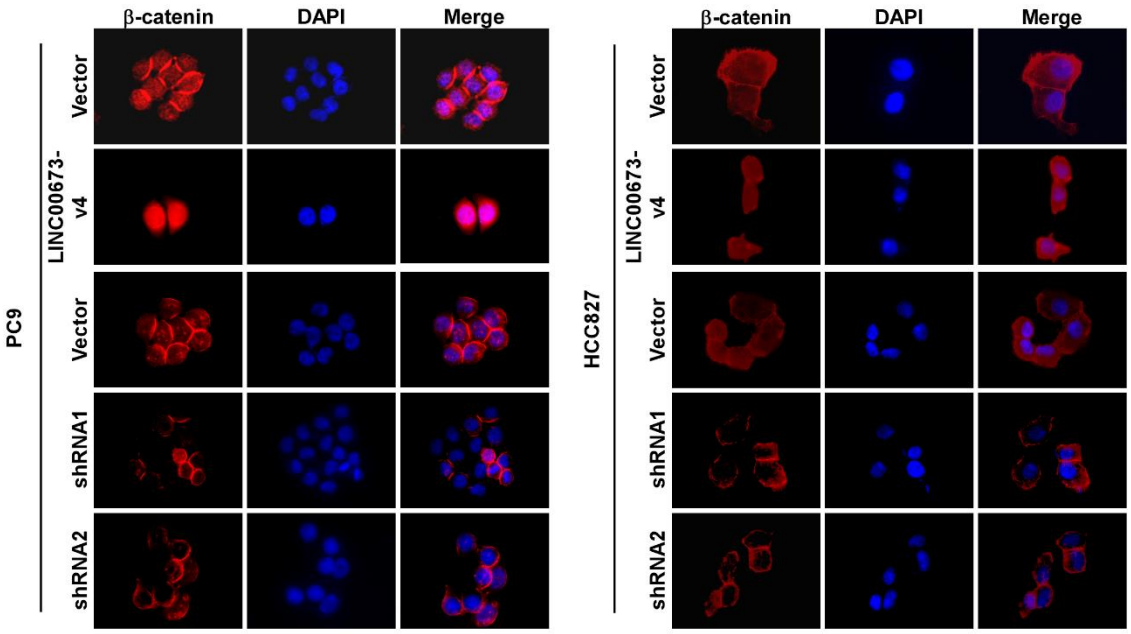

Fig. S8. Subcellular β-catenin localization in indicated cells.

Subcellular β-catenin localization was assessed using immunofluorescence staining and representative images are shown.

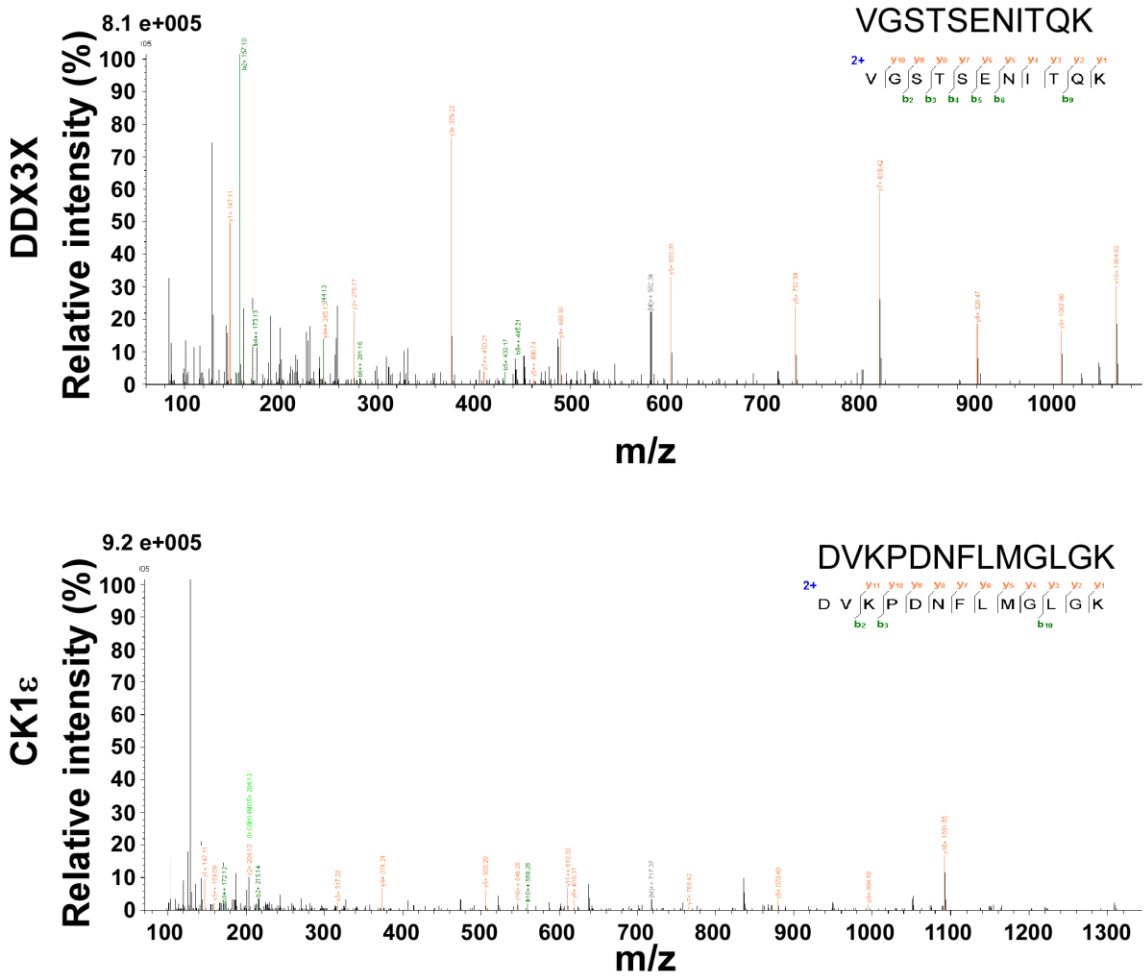

Fig. S9. The mass spectrum analysis of specific bands.

Specific bands were identified by mass spectrum.

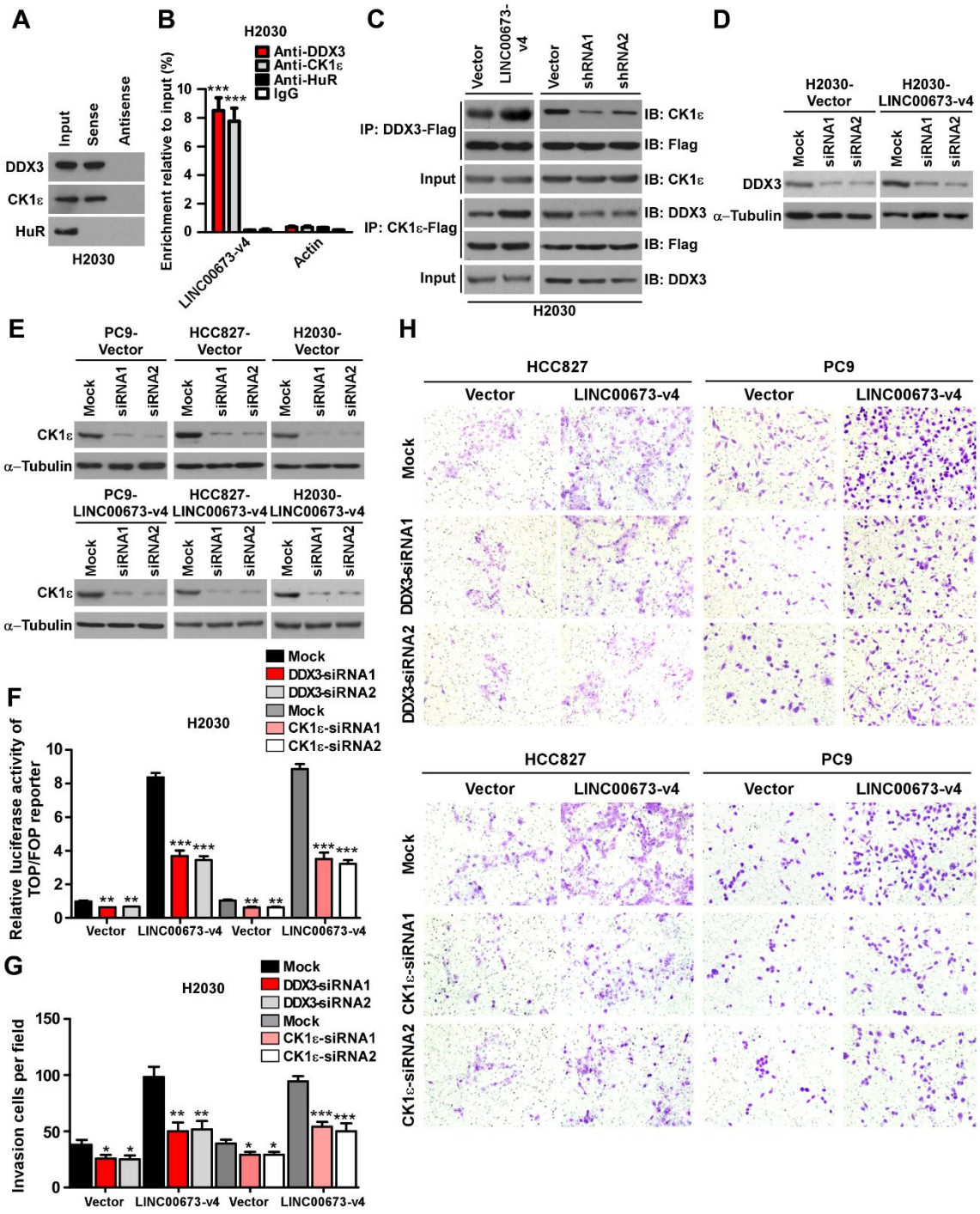

Fig. S10. LINC00673-v4 interacts with DDX3 and CK1ε.

(A) RNA pull-down experiment followed by WB analysis of LINC00673-v4 interactional proteins in H2030 cells. (B) RIP assays after UV crosslink analyzed the interaction of LINC00673-v4 with DDX3 and CK1ε (each bar represents the mean ± SD derived from

three experiments, one-way ANOVA followed by Dunnett's multiple comparison test. ***$P < 0.001$). (C) Co-IP detection of the indicated proteins in indicated cells with LINC00673-v4 overexpression or knockdown. (D and E) WB analysis of the transfection of siCK1ε (D) or siDDX3 (E) in LINC00673-v4-overexpressing and vector-control LAD cells. (F) Luciferase analysis of TCF/LEF transcriptional activity in indicated cells (each bar represents the mean ± SD derived from three experiments, one-way ANOVA followed by Dunnett's multiple comparison test. **$P < 0.01$, ***$P < 0.001$). (G) Quantification of invading cells using the Transwell invasion assay in LINC00673-v4-overexpressing and vector-control cells with depletion of CK1ε or DDX3 (each bar represents the mean ± SD derived from three experiments, one-way ANOVA followed by Dunnett's multiple comparison test. *$P < 0.05$, **$P < 0.01$, ***$P < 0.001$). (H) Representative micrographs of indicated invading cells analyzed by Matrigel-coated Transwell assay.

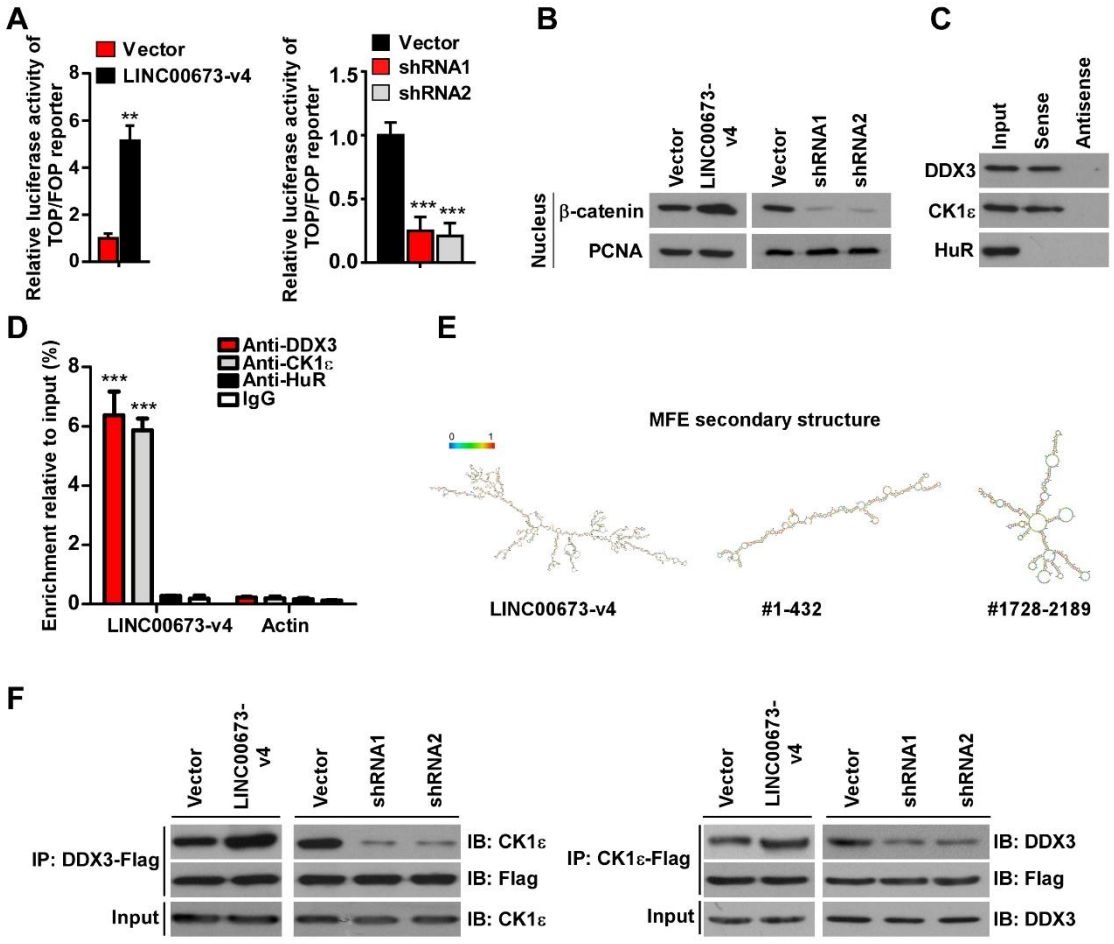

Fig. S11. LINC00673-v4 enhances the interaction of DDX3 and CK1ε in patient-derived LAD cells.

(A) The activity of Wnt/β-catenin signaling was analyzed by TOP/FOP luciferase activity assay (left: each bar represents the mean ± SD derived from three independent experiments, two-tailed Student's t test; right: each bar represents the mean ± SD derived from three experiments, one-way ANOVA followed by Dunnett's multiple comparison test. $^{**}P < 0.01$, $^{***}P < 0.001$). (B) Altered nuclear translocation of β-catenin were analyzed by WB analysis. PCNA was used as a loading control. (C) WB analysis data show binding of LINC00673-v4 with DDX3 and CK1ε. (D) RIP assays were performed to verify the interaction of LINC00673-v4 with DDX3 and CK1ε (each bar represents the

mean ± SD derived from three experiments, one-way ANOVA followed by Dunnett's multiple comparison test. ***$P < 0.001$). (E) Two binding fragments with stable stem-loop structures predicted by RNA folding analysis. (F) Co-IP detection of the indicated proteins in indicated cells with LINC00673-v4 overexpression or knockdown.

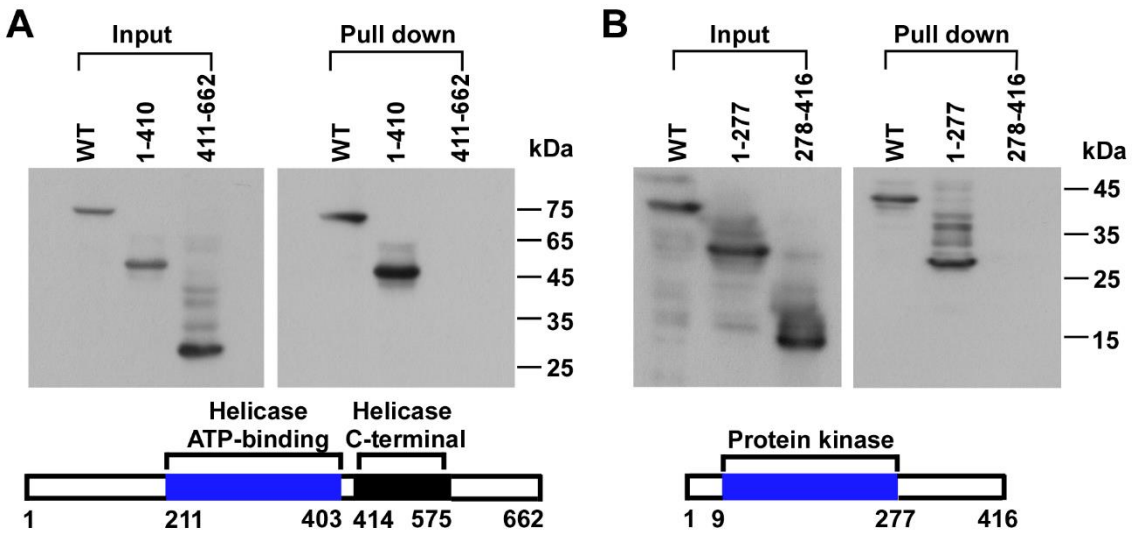

Fig. S12. The helicase ATP-binding domain of DDX3 and the protein kinase domain of CK1ε interacts with LINC00673-v4.

(A and B) WB analysis of FLAG-tagged domain truncation mutants of DDX3 (A) and CK1ε (B) retrieved by LINC00673-v4. The domain structure of DDX3 and CK1ε was shown below, respectively.

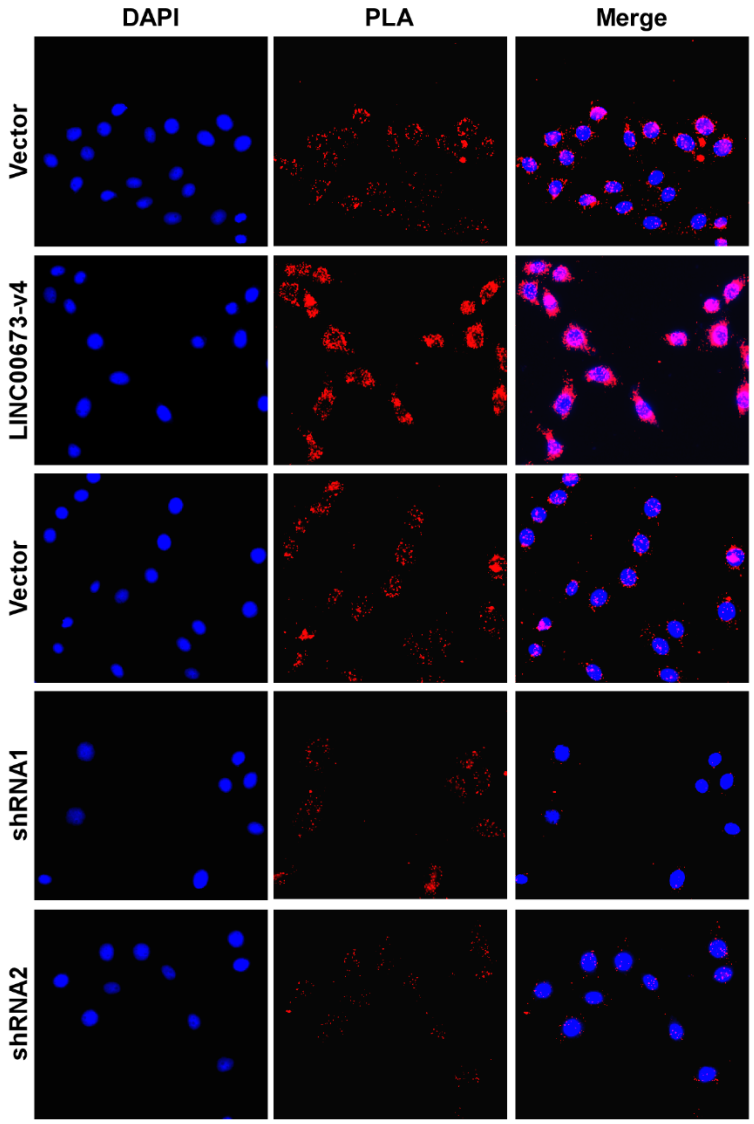

Fig. S13. The interaction between DDX3 and CK1ε.

In situ Proximity Ligation Assay was performed to assess the interaction between DDX3 and CK1ε.

Table S1. LINC00673-v4 is located within a chromosomal region commonly amplified in NSCLC

Amplified Region	Residual Q-value	Overall Frequency of Amplification
Chr17:55353997-78605474	0.128	0.396

Data are taken from The Broad Institute's Tumorscape database (Nature. 2010; 463:899-905)

Table S2. Clinicopathologic characteristics of LAD patients from SYSUCC cohort

Characteristics	Number of cases	Percentage
Gender		
Male	81	68.1%
Female	38	31.9%
Age (years)		
>60	44	37.0%
≤60	75	63.0%
Clinical Stage		
I + II	67	56.3%
III+ IV	52	43.7%
T classification		
T1 + T2	84	70.6%
T3 + T4	35	29.4%
N classification		
N0	57	47.9%
N1	25	21.0%
N2	35	29.4%
N3	2	1.7%
Distant metastasis		
Yes	6	5.0%
No	113	95.0%

Table S3. Correlation between expressions of LINC00673-v4 and clinicopathologic features in LAD patients from SYSUCC cohort

Characteristics	cutoff	Below cutoff N	Above cutoff N	P-value
Gender				
Male	13.996	62	19	0.071
Female		23	15	
Age				
>60	10.320	12	32	0.093
≤ 60		32	43	
Clinical stage				
I + II	11.008	37	30	0.014
III+ IV		17	35	
T classification				
T1+T2	17.455	76	8	0.021
T3+T4		26	9	
LN metastasis				
Yes	11.970	27	35	0.006
No		39	18	
Distant metastasis				
Yes	13.079	3	3	0.498
No		72	41	

Table S4. Correlation between the clinicopathological features and LINC00673 CNV status in LAD patients from SYSCUU cohort

Characteristics	LINC673 CNV status		*P*-value
	non-Amp	Amp	
Gender			
Male	68	13	0.102
Female	27	11	
Age (years)			
>60	37	7	0.375
≤ 60	58	17	
Clinical stage			
I + II	60	7	0.003
III + IV	35	17	
T classification			
T1 + T2	67	17	0.976
T3 + T4	28	7	
LN metastasis			
Yes	42	20	0.001
No	53	4	
Distant metastasis			
Yes	4	2	0.410
No	91	22	

Table S5. Clinicopathologic characteristics of LAD patients from TCGA Dataset

Characteristics	Number of cases	Percentage
Gender		
Male	169	49.4%
Female	173	50.6%
Age (years)		
>60	220	64.3%
≤60	103	30.1%
Unknown	19	5.6%
Clinical stage		
I+II	259	75.7%
III+IV	83	24.3%
T classification		
T1+ T2	297	86.8%
T3+ T4	45	13.2%
N classification		
N0	212	62.0%
N1	73	21.3%
N2	56	16.4%
N3	1	0.3%
Distant metastasis		
Yes	20	5.8%
No	322	94.2%

Table S6. Correlation between expressions of LINC00673 and clinicopathologic features in LAD patients from TCGA Dataset

Characteristics	cutoff	Below cutoff N	Above cutoff N	P-value
Gender				
Male	1.590	76	93	0.399
Female		70	103	
Age				
>60	2.690	154	66	0.104
≤ 60		81	22	
unknown		19		
Clinical stage				
I + II	2.030	147	112	0.120
III+ IV		39	44	
T classification				
T1+T2	3.859	265	32	0.000
T3+T4		5	40	
LN metastasis				
Yes	0.898	19	111	0.002
No		62	150	
Distant metastasis				
Yes	0.344	1	19	0.592
No		27	295	

Table S7. List of LINC00673-v4 interacting proteins identified by mass spectrometry in band 1

Protein	Entry name	Gene name	Unique peptides
P52272	HNRPM_HUMAN	HNRPM	22
P02545	LMNA_HUMAN	LMNA	15
Q59F66	Q59F66_HUMAN	DDX17	6
P11021	GRP78_HUMAN	GRP78	4
O43390	HNRPR_HUMAN	HNRPR	3
Q5SSJ5	HP1B3_HUMAN	HP1BP3	3
A0A0D9SF53	A0A0D9SF53_HUMAN	DDX3X	2
Q15061	WDR43_HUMAN	WDR43	2
Q5BKZ1	ZN326_HUMAN	ZNF326	2
H0YAR2	H0YAR2_HUMAN	H0YAR2	2

Table S8. List of LINC00673-v4 interacting proteins identified by mass spectrometry in band 2

Protein	Entry name	Gene name	Unique peptides
Q9HCC0	MCCB_HUMAN	MCCC2	31
P14618	KPYM_HUMAN	PKM	31
P35527	K1C9_HUMAN	KRT9	29
P04264	K2C1_HUMAN	KRT1	24
Q9H078	CLPB_HUMAN	CLPB	24
P26599	PTBP1_HUMAN	PTBP1	21
P13645	K1C10_HUMAN	KRT10	16
Q15233	NONO_HUMAN	NONO	16
P09914	IFIT1_HUMAN	IFIT1	15
O75131	CPNE3_HUMAN	CPNE3	14
O14879	IFIT3_HUMAN	IFIT3	14
P11413	G6PD_HUMAN	G6PD	14
P04745	AMY1_HUMAN	AMY1A	13
P40227	TCPZ_HUMAN	CCT6A	13
P26368	U2AF2_HUMAN	U2AF2	12
Q9Y450	HBS1L_HUMAN	HBS1L	12
P12268	IMDH2_HUMAN	IMPDH2	10
P68363	TBA1B_HUMAN	TUBA1B	10
Q9UHR4	BI2L1_HUMAN	BAIAP2L1	9
O43143	DHX15_HUMAN	DHX15	9
Q99832	TCPH_HUMAN	CCT7	9
P07237	PDIA1_HUMAN	P4HB	9
P61978	HNRPK_HUMAN	HNRNPK	8
P02489	CRYAA_HUMAN	CRYAA	8
O43776	SYNC_HUMAN	NARS	8
P17844	DDX5_HUMAN	DDX5	8
Q8WWY3	PRP31_HUMAN	PRPF31	8
O43175	SERA_HUMAN	PHGDH	8
Q13325	IFIT5_HUMAN	IFIT5	7
Q9UN86	G3BP2_HUMAN	G3BP2	7
P11940	PABP1_HUMAN	PABPC1	6
P60709	ACTB_HUMAN	ACTB	6
P63261	ACTG_HUMAN	ACTG1	6
P25705	ATPA_HUMAN	ATP5A1	5
P01876	IGHA1_HUMAN	IGHA1	5
Q8WU90	ZC3HF_HUMAN	ZC3H15	5
Q13501	SQSTM_HUMAN	SQSTM1	5
P13647	K2C5_HUMAN	KRT5	4
P50991	TCPD_HUMAN	CCT4	4

P05109	S10A8_HUMAN	S100A8	4
P31948	STIP1_HUMAN	STIP1	4
O60701	UGDH_HUMAN	UGDH	4
Q8N684	CPSF7_HUMAN	CPSF7	4
Q96GM8	TOE1_HUMAN	TOE1	4
P68104	EF1A1_HUMAN	EEF1A1	3
Q5VTE0	EF1A3_HUMAN	EEF1A1P5	3
Q05639	EF1A2_HUMAN	EEF1A2	3
P02768	ALBU_HUMAN	ALB	3
P01834	IGKC_HUMAN	IGKC	3
P06576	ATPB_HUMAN	ATP5B	3
P06702	S10A9_HUMAN	S100A9	3
P14866	HNRPL_HUMAN	HNRNPL	3
Q08211	DHX9_HUMAN	DHX9	3
P19525	E2AK2_HUMAN	EIF2AK2	3
Q9UHD8	SEPT9_HUMAN	SEPT9	3
P01833	PIGR_HUMAN	PIGR	3
Q96A33	CCD47_HUMAN	CCDC47	3
Q9BUJ2	HNRL1_HUMAN	HNRNPUL1	3
P62805	H4_HUMAN	HIST1H4A	3
P36578	RL4_HUMAN	RPL4	3
Q8NC51	PAIRB_HUMAN	SERBP1	3
P09228	CYTT_HUMAN	CST2	2
P07437	TBB5_HUMAN	TUBB	2
P31943	HNRH1_HUMAN	HNRNPH1	2
Q13310	PABP4_HUMAN	PABPC4	2
P68371	TBB4B_HUMAN	TUBB4B	2
P19338	NUCL_HUMAN	NCL	2
P0CF74	IGLC6_HUMAN	IGLC6	2
P0DOY2	IGLC2_HUMAN	IGLC2	2
P0DOY3	IGLC3_HUMAN	IGLC3	2
P05455	LA_HUMAN	SSB	2
P12273	PIP_HUMAN	PIP	2
P35637	FUS_HUMAN	FUS	2
P23280	CAH6_HUMAN	CA6	2
Q9NUQ6	SPS2L_HUMAN	SPATS2L	2
P06744	G6PI_HUMAN	GPI	2
Q9ULV4	COR1C_HUMAN	CORO1C	2
O60832	DKC1_HUMAN	DKC1	2
P01859	IGHG2_HUMAN	IGHG2	2
P01861	IGHG4_HUMAN	IGHG4	2
Q9Y6M1	IF2B2_HUMAN	IGF2BP2	2
Q9UJA5	TRM6_HUMAN	TRMT6	2
Q9UQB8	BAIP2_HUMAN	BAIAP2	2

P78371	TCPB_HUMAN	CCT2	2
Q9NRG9	AAAS_HUMAN	AAAS	2
Q02790	FKBP4_HUMAN	FKBP4	2
O00505	IMA4_HUMAN	KPNA3	2
P16989	YBOX3_HUMAN	YBX3	2

Table S9. List of LINC00673-v4 interacting proteins identified by mass spectrometry in band 3

Protein	Entry name	Gene name	Unique peptides
P06576	ATPB_HUMAN	ATP5B	23
P00367	DHE3_HUMAN	GLUD1	23
P25705	ATPA_HUMAN	ATP5A1	21
P35527	K1C9_HUMAN	KRT9	21
P13645	K1C10_HUMAN	KRT10	19
P05166	PCCB_HUMAN	PCCB	19
P05787	K2C8_HUMAN	KRT8	19
P68104	EF1A1_HUMAN	EEF1A1	18
P14868	SYDC_HUMAN	DARS	18
Q05639	EF1A2_HUMAN	EEF1A2	17
P04264	K2C1_HUMAN	KRT1	14
P05455	LA_HUMAN	SSB	14
Q9Y230	RUVB2_HUMAN	RUVBL2	14
P62495	ERF1_HUMAN	ETF1	14
Q9H0S4	DDX47_HUMAN	DDX47	13
P35908	K22E_HUMAN	KRT2	12
P04745	AMY1_HUMAN	AMY1A	12
P36578	RL4_HUMAN	RPL4	12
P26641	EF1G_HUMAN	EEF1G	12
O95793	STAU1_HUMAN	STAU1	12
Q96CW1	AP2M1_HUMAN	AP2M1	12
Q9P0V9	SEP10_HUMAN	SEPT10	11
P31943	HNRH1_HUMAN	HNRNPH1	10
Q9NVA2	SEP11_HUMAN	SEPT11	9
Q9UMS4	PRP19_HUMAN	PRPF19	9
Q9Y265	RUVB1_HUMAN	RUVBL1	8
P02489	CRYAA_HUMAN	CRYAA	8
Q9Y3I0	RTCB_HUMAN	RTCB	8
Q9BUF5	TBB6_HUMAN	TUBB6	7
P04637	P53_HUMAN	TP53	7
Q96P11	NSUN5_HUMAN	NSUN5	7
P51648	AL3A2_HUMAN	ALDH3A2	7
P55795	HNRH2_HUMAN	HNRNPH2	6
Q2VIR3	IF2GL_HUMAN	EIF2S3L	6
P41091	IF2G_HUMAN	EIF2S3	6
Q8NCE0	SEN2_HUMAN	TSEN2	6
P19338	NUCL_HUMAN	NCL	6
P07437	TBB5_HUMAN	TUBB	5
P60709	ACTB_HUMAN	ACTB	5
P63261	ACTG_HUMAN	ACTG1	5

Q14974	IMB1_HUMAN	KPNB1	5
O00148	DX39A_HUMAN	DDX39A	5
P68366	TBA4A_HUMAN	TUBA4A	4
Q14141	SEPT6_HUMAN	SEPT6	4
Q92599	SEPT8_HUMAN	SEPT8	4
Q86U42	PABP2_HUMAN	PABPN1	4
Q9UKS6	PACN3_HUMAN	PACSIN3	4
P18754	RCC1_HUMAN	RCC1	4
Q9NQC3	RTN4_HUMAN	RTN4	4
P12081	SYHC_HUMAN	HARS	4
Q9H814	PHAX_HUMAN	PHAX	4
Q16576	RBBP7_HUMAN	RBBP7	4
Q9P258	RCC2_HUMAN	RCC2	4
Q9NUL3	STAU2_HUMAN	STAU2	4
P13647	K2C5_HUMAN	KRT5	3
P01876	IGHA1_HUMAN	IGHA1	3
P48730	KC1D_HUMAN	CSNK1D	3
P49674	KC1E_HUMAN	CSNK1E	3
Q12849	GRSF1_HUMAN	GRSF1	3
P26196	DDX6_HUMAN	DDX6	3
Q92989	CLP1_HUMAN	CLP1	3
Q8IZP2	ST134_HUMAN	ST13P4	3
P50502	F10A1_HUMAN	ST13	3
O60825	F262_HUMAN	PFKFB2	3
Q15084	PDIA6_HUMAN	PDIA6	3
P13639	EF2_HUMAN	EEF2	3
P62805	H4_HUMAN	HIST1H4A	3
Q7L5N7	PCAT2_HUMAN	LPCAT2	3
P01833	PIGR_HUMAN	PIGR	3
P0CG12	CTF8A_HUMAN	CHTF8	3
Q9NR50	EI2BG_HUMAN	EIF2B3	3
Q9BQE3	TBA1C_HUMAN	TUBA1C	2
Q13509	TBB3_HUMAN	TUBB3	2
P02768	ALBU_HUMAN	ALB	2
P09228	CYTT_HUMAN	CST2	2
P01834	IGKC_HUMAN	IGKC	2
Q16658	FSCN1_HUMAN	FSCN1	2
P05109	S10A8_HUMAN	S100A8	2
P36957	ODO2_HUMAN	DLST	2
Q8IUF8	MINA_HUMAN	MINA	2
P23280	CAH6_HUMAN	CA6	2
Q9NW64	RBM22_HUMAN	RBM22	2
P11413	G6PD_HUMAN	G6PD	2
Q8N1N4	K2C78_HUMAN	KRT78	2

Table S10. List of LINC00673-v4 interacting proteins identified by mass spectrometry in band 4

Protein	Entry name	Gene name	Unique peptides
P49674	KC1E_HUMAN	CSNK1E	17
P04745	AMY1_HUMAN	AMY1A	10
P36578	RL4_HUMAN	RPL4	10
P13645	K1C10_HUMAN	KRT10	8
P07437	TBB5_HUMAN	TUBB	8
P04264	K2C1_HUMAN	KRT1	7
P26641	EF1G_HUMAN	EEF1G	7
P02489	CRYAA_HUMAN	CRYAA	7
P68104	EF1A1_HUMAN	EEF1A1	6
P35908	K22E_HUMAN	KRT2	5
Q05639	EF1A2_HUMAN	EEF1A2	4
P35527	K1C9_HUMAN	KRT9	4
P41091	IF2G_HUMAN	EIF2S3	4
P11142	HSP7C_HUMAN	HSPA8	3
P08779	K1C16_HUMAN	KRT16	3
P12273	PIP_HUMAN	PIP	3
P60709	ACTB_HUMAN	ACTB	3
P63261	ACTG_HUMAN	ACTG1	3
P06733	ENOA_HUMAN	ENO1	3
P01876	IGHA1_HUMAN	IGHA1	3
P20042	IF2B_HUMAN	EIF2S2	3
P02538	K2C6A_HUMAN	KRT6A	2
P13647	K2C5_HUMAN	KRT5	2
P09228	CYTT_HUMAN	CST2	2
P01834	IGKC_HUMAN	IGKC	2
P81605	DCD_HUMAN	DCD	2
P23280	CAH6_HUMAN	CA6	2

Table S11. Spearman correlation analysis between LINC00673-v4 level and expression of nuclear β-catenin, Twist, HOXB9, MMP9, and VEGF

Variables	LINC00673-v4	
	Spearman correlation	*P*
Nuclear β-catenin	0.238	0.009
TWIST	0.205	0.025
HOXB9	0.197	0.032
MMP9	0.191	0.038
VEGF	0.202	0.028

Table S12. SiRNA sequences

Target gene	Sequences (5’ to 3’)
LINC00673-1	CCAGUGUGUGCUGAUGACACAUACA
LINC00673-2	GCUUUCUACCACACCCUUUCU
CK1ε-1	CAACAUACCUCAACUUCUG
CK1ε-2	GAGCAAAGCCGUCGAGAUG
DDX3X-1	CGAGAGAGUUGGCAGUACA
DDX3X-2	CAUUGAGCUUACUCGUUAU
LEF1-1	GUUAUUCCGGGUACAUAAU
LEF1-2	UCAGAUGUCAACUCCAAACAA
TCF4-1	AAGUCCGAGAAAGGAAUCUGA
TCF4-2	GAACCUAUCUCCAGAUGAAUU

Table S13. Primers for RACE analysis

Primer name	Sequences (5' to 3')
5' RACE-1	AAGCACCCACCGAGTCAGCCAGAAACCT
5' RACE-2	GGTTTCTGGCTGACTCGGTGGGTGCTTT
3' RACE-1	GAGACAGGGTCTCTCGCTCTTTTGCCCA
3' RACE-2	GGAGAATAAAGAGACCTCTGGATTTGAG

Table S14. Primer sequences for qRT-PCR

Target gene	Sequences (5' to 3')
LINC00673-V1	Forward: ATTTTTCCCTCTCCACCCTGG
	Reverse: CCAGCCCTGTAGAGGTCCTCA
LINC00673-V2	Forward: CAAGCTGGAGGTGGAATCAGAGG
	Reverse: AGGAGGTGGCACCTCTTTCTTG
LINC00673-V3	Forward: ATTTTTCCCTCTCCACCCTGG
	Reverse: GTCCTTCCCATCCTCTTTCTTG
LINC00673-V4	Forward: CAAGCTGGAGGTGGAATCAGAGG
	Reverse: GTCCTTCCCATCCTCTTTCTTG
LINC00673-V5	Forward: AGATCAGGTTCAAGTTGCCAG
	Reverse: CTGCAGGGCCGGGAGGAGAGG
HOXB9	Forward: TCCAGCGTCTGGTATTTGGT
	Reverse: GAAGCGAGGACAAAGAGAGG
Twist	Forward : TCCATTTTCTCCTTCTCTGGAA
	Reverse: GTCCGCGTCCCACTAGC
MMP9	Forward :ACGACGTCTTCCAGTACCGA
	Reverse :TTGGTCCACCTGGTTCAACT
VEGF	Forward: CTACCTCCACCATGCCAAGT
	Reverse: AGCTGCGCTGATAGACATCC
ACTB	Forward: GTTGTCGACGACGAGCG
	Reverse: GCACAGAGCCTCGCCTT
U6	Forward: CTCGCTTCGGCAGCACA
	Reverse: AACGCTTCACGAATTTGCGT
GAPDH	Forward: GACTCATGACCACAGTCCATGC
	Reverse: AGAGGCAGGGATGATGTTCTG
LINC0673	Forward: CTCATTGACCTGCACGAAGA
-CNV	Reverse: AGCTCACATCGTCAGGCTTT
LINE-1-CNV	Forward: AAAGCCGCTCAACTACATGG
	Reverse: TGCTTTGAATGCGTCCCAGAG

Table S15. Probe sequence used in ISH and Northern blot analysis

Probe name	Probe sequence (5' to 3')
Probe	CTGCTTGCAACACACAAACACT

References

1. Cai J, et al. (2017) Simultaneous overactivation of Wnt/beta-catenin and TGFbeta signalling by miR-128-3p confers chemoresistance-associated metastasis in NSCLC. *Nat Commun* 8:15870.
2. Pecze L, Blum W, Schwaller B (2015) Routes of Ca2+ Shuttling during Ca2+ Oscillations: FOCUS ON THE ROLE OF MITOCHONDRIAL Ca2+ HANDLING AND CYTOSOLIC Ca2+ BUFFERS. *J Biol Chem* 290(47):28214-28230.
3. Liu L, et al. (2017) Astrocyte Elevated Gene 1 Interacts with Acetyltransferase p300 and c-Jun To Promote Tumor Aggressiveness. *Mol Cell Biol* 37(5).
4. Okudela K, et al. (2007) PIK3CA mutation and amplification in human lung cancer. *Pathol Int* 57(10):664-671.
5. Jiang L, et al. (2012) MicroRNA-30e* promotes human glioma cell invasiveness in an orthotopic xenotransplantation model by disrupting the NF-kappaB/IkappaBalpha negative feedback loop. *J Clin Invest* 122(1):33-47.
6. Gomez-Martin C, et al. (2013) Level of HER2 gene amplification predicts response and overall survival in HER2-positive advanced gastric cancer treated with trastuzumab. *J Clin Oncol* 31(35):4445-4452.
7. Zlobec I, et al. (2007) A simple and reproducible scoring system for EGFR in colorectal cancer: application to prognosis and prediction of response to preoperative brachytherapy. *Br J Cancer* 96(5):793-800.
8. Dumbovic G, et al. (2018) A novel long non-coding RNA from NBL2 pericentromeric macrosatellite forms a perinucleolar aggregate structure in colon cancer. *Nucleic Acids Res* 46(11):5504-5524.
9. Li J, et al. (2010) Oncoprotein Bmi-1 renders apoptotic resistance to glioma cells through activation of the IKK-nuclear factor-kappaB Pathway. *Am J Pathol* 176(2):699-709.